Monte Carlo study of the Higgs boson in the decay channels $H \rightarrow W^+W^- \rightarrow 2\mu\, 2\nu_\mu$ and $H \rightarrow Z^0Z^0 \rightarrow 4\mu$

Luis Emiro Linares García

Thesis submitted for
the Degree of Physicist

Director
Carlos Arturo Ávila Bernal, Ph.D.

Universidad de los Andes
Department of Physics
Bogotá D.C.
November 2007

In memory of all the giants on which
one can stand to view
the vast extent of Nature

A mis padres, quienes son Amor,
soporte y apoyo en todas mis empresas.
A mi familia, que me alegra la existencia.
A mis amigos, quienes extienden
mi experiencia de la misma.

Abstract

In this thesis work we study the production and decay of the Standard Model Higgs Boson in the weak decay modes, which consequently branch to muonic final states (muons and muonic neutrinos). The physics scenario is the LHC (two protons colliding with a center-of-mass energy of 14 TeV). Only Physics simulation is performed, with no detector simulation. We study discovery possibilities by effecting kinematic cuts on the data, and also by using a neural network to try to enhance the resulting Signal-to-Noise Ratio.

Contents

List of Figures

Introduction

Through all the years of its existence, the Standard Model has done nothing but fulfilling expectations and successfully predicted phenomena related to how fundamental interactions behave and relate. Up to this moment, the Standard Model has correctly given account of the number of fermions and bosons that make up the world we see.

What is precisely the Standard Model? It is a compact collection of the concepts through which we describe physics at the elementary particle level. This compact collection entails the description of matter made by a set of quarks and leptons, interacting with each other by exchange of another set of gauge bosons. In the tables 1 and 2 the current underlying structure of the subatomic world is set, as it is dictated by the Standard Model.

Particles	**Generations**		
	One	**Two**	**Three**
Quarks	u, d	s, c	t, b
Leptons	e, ν_e	μ, ν_μ	τ, ν_τ

Table 1: Elementary Particles of the Standard Model

Interaction	**Mediators**	**Participants**
Electroweak	bosons γ, $W^{\pm}$, Z^0	quarks and leptons
Strong	Gluons g	quarks
Gravitational	Graviton G	All of above

Table 2: Interactions of the Standard Model

This rather simple structure has been able to account for the myriad of particles that are visible in, for example, a bubble chamber, as well as for the matter we're all made of, as composites of 3 quarks (called baryons) or quark-antiquark pairs (called mesons). It describes rather accurately different phenomena like the decay of the neutron (which

is responsible for radioactivity), the effects of vaccum polarization on atomic spectra, etc. Despite its long list of milestones, there's still a missing piece which is fundamental for its mathematical and physical consistency: the Higgs boson. For the mathematical consistency, it is a direct consequence of the mathematical structure of the Standard Model, and for the physical congruity, it is the mechanism that gives rise to the mass of particles. This sole fact makes it a validation or rejection method for the Standard Model, as its non-discovery would force us to move to other directions in the search for the theory of elementary paticles and interactions.

The experimental activity within the Standard Model began around the middle of the XX century, and in particular the search for the Higgs boson started at LEP, the Large Electron-Proton collider at CERN, after 1989, when it went into operation. Several other high energy facilities around the world have also contributed to this search. In spite of so much years and efforts in this search, this particle has eluded discovery. At present, the LEP experiments have constrained the mass of the Higgs boson with a lower bound of 114.4 $\mathrm{GeV}/\mathrm{c}^2$. The next steps in this direction are to be taken in the LHC, which is due to begin operation on 2008. With a wider accesible region of phase and parameter space, any undiscovered physics is highly likely to be found in the experiments performed in this $p - p$, 14 TeV collider. Therefore, our study focuses on the simulation of SM Higgs processes generated by the collision of protons at 14 TeV Center-of-Mass energy, as a way to get a glimpse at what might be seen at the machine when it begins operation.

This work is organized as follows: We first briefly outline of the structure of the Standard Model (chapter 1), with an emphasis on the Electroweak Symmetry Breaking mechanism that underlies on this conceptual body. Then we show the experimental efforts regarding the Higgs search, in particular, the constraints obtained from electroweak parameter precision measurements and direct searches by several Higgs working groups (chapter 2); Next, we outline the computational setup used in the development of this thesis, detailing the programs used and the purpose of each within our work (chapter 3), all of them resulting in the data we present and analyze in chapter 4, after which we present our conclusions. Throughout the document, distributed as is necessary, the results of the two Monte Carlo programs are compared on figures that contrast the differences.

Chapter 1

The Standard Model

In this chapter we present the structure of the Standard Model, with views to discuss the mechanism of Electroweak Symmetry Breaking. We then discuss the Higgs mechanism and some of its features, specially those related to ways of detect it.

The Standard Model describes matter as compound of quarks and leptons. These are two families of spin-1/2 particles (fermions), each one with 6 members, categorized in three generations (and, of course, for each particle there exists also its associated antiparticle). For the leptons, we have the electron, the muon and the tau, each one with an associated massless [1] neutrino, which carries no electric or any other charge. For the massive members of this family, the only stable one is the electron, with the others ones decaying mainly in electrons and neutrinos, but the tau has also hadronic decay modes. For the quarks, all of them are massive and have fractional electric charge. They are put on the Table 1. The letters stand for *Up*, *Down*, *Strange*, *Charm*, *Top*, *Bottom* (or *Truth* and *Beauty*).

For the interactions, it is interesting to see how they were recognized and included in the theory. The first of them is the electromagnetic interaction, which still today remains as the most successful example of phenomena unification. Before the electromagnetic theory, there were a number of disconnected, even tough similar, formulations of electric and magnetic variables, and there was the idea of an invisible ubiquitous medium through which light would propagate. Then Maxwell published his legendary *Treatise on Electricity and Magnetism* in which he accounted for all the available knowledge in electricity and magnetism in just four vector equations, which through a simple set of transformations yields the equation of a wave propagating at the speed of light, measured with respect to no particular reference frame. And so this first act of unification of physical theories, with time and work, gave rise to two strongly fundamental facts: Light is an electromagnetic wave, and Special Relativity. Later, with the immersion of Quantum Mechanics in the landscape of Physics, a quantum theory

[1] This was only in principle, as the recent observation of neutrino oscillations implied that neutrinos have a very small, but nonetheless non-zero, mass.

of the covariant formulation of electromagnetism arose, known as Quantum Electrodynamics (QED), with spectacular achievements like the prediction of the hyperfine structure of the Hydrogen atom, described as the effect on the atom of spontaneous creation and annihilation of electron-positron pairs out of the polarized vacuum.

After the conception of the quarks as the composers of all the observed hadrons (this one is beautiful story, but also a long one, so we only recommend the interested reader to read, for example, [16]), the observation of bound states of three identical-flavor quarks (for example, the Σ^- baryon made of three strange quarks) revolutionized the physics community, because that fact would violate the Fermi Exclusion Principle (all three quarks would be in the same state). However, this would not be the case if there exists another physical property of the quarks that made each of them unidentical within the bound state. It has somehow to be unobservable to us in the experiment, because othewise we would have noticed and a new way to classify particles would be known. This new physical property is now known as the color charge, inspired in analogy to the way colors mix, with red, green and blue, and also red with cyan (anti-red), blue with yellow (anti-blue) and green with magenta (anti-green), all mixing to yield white. The two-color mixes would apply to mesons (with the quark carrying a color and the antiquark carrying the anticolor) and the three-color mix for baryons (each quark with a different color), so that all the physical states we observe have to be "white" [2]. We will soon see, the color interaction makes part of the symmetry group which represents the dynamics of the Standard Model. As a Quantum Field Theory like QED, it is known as Quantum Chromodynamics (QCD).

The unusually large time a neutron takes to decay into a proton, an electron and a "missing energy" (around 15 minutes!) could not be accounted by an electromagnetic or strong process, as strong decays have a typical lifetime of 10^{-23} seconds. This decay (observed as the beta decay of radioactive nuclei) also challenged physicists with an unusual and at first very shocking feature: the measured energy distribution of the produced electron was not a sharp spike at the value enforced by energy conservation (by assumming a decay to two particles), but had a spread spectrum. These two striking facts signaled the presence of a new fundamental interaction, and following Fermi's development of a theory of the weak interaction with no propagators, only a point vertex, and several other relevant works, a theory of weak interactions with vector and axial couplings (to account for parity violation as it was evidenced in experiments with cobalt-60 atoms) to three massive gauge bosons was developed, ending with the unified electroweak scheme developed by Sheldon Glashow, Stephen Weinberg and Abdus Salam, which describes the electromagnetic and weak forces as manifestations of a single interaction, which is mediated by four spin-1 bosons.

[2] Even tough the analogy is so compelling, it is very important to clarify there is no connection at all with light and electromagnetism

To this nice picture of successful descriptions of matter at the subatomic level unfortunately we have to add several "kinks", failures and shortcomings it presents, the ones which also make present and future physics research relevant and necessary to approach every time closer to the full insight of Nature's workings. As for the shortcomings, the most important one is the exclusion of gravity from the description, goal which at present still resists victory. The other very notorious one is the unknown principle for the rather big differences in the mass of the particles, and also in the magnitudes of the strength of the interactions. That means, for one part, the origin of mass is not clear, and for the other, the idea of a complete unification of forces is not feasible within the theory. With regard to the origin of mass, Peter Higgs pointed out a mechanism by which the electroweak symmetry is broken, giving rise to three massive bosons (Z^0 and $W^{\pm}$) and a massless one (the photon). This mechanism reveals itself as a massive scalar particle, whose associated field permeates all the Universe, which couples to the particles with a strength proportional to each particle's mass, which would show the Higgs boson as the originator of mass. However, the theory does not predict the mass of the Higgs, and only contraints from renormalizability, unitarity restrictions on weak boson scattering amplitudes and the requirement that its total decay width be less than its mass can be used to get limits on the allow ranged of values for this property[11].

1.1 The Standard Model Lagrangian

1.1.1 The Gauge/Fermion component

More formally, the Standard Model is a Yang-Mills theory with symmetry group $SU(2)_L \times U(1)_Y \times SU(3)_C$, where the L represents chiral couplings to left-handed fermions, Y the weak hypercharge and C the color charge, each of them representing the weak, electromagnetic[3] and color interactions, respectively. The Lagrangian for a Yang-Mills theory has the general form[10]:

$$\mathcal{L}_{\mathrm{Y-M}} = i\bar{\eta}\gamma_\mu D^\mu \eta - \frac{1}{4} F^a_{\nu\mu} F^{a\nu\mu} \tag{1.1}$$

where the D^μ is the covariant derivative that specifies interactions, $igF_{\mu\nu} = [D_\mu, D_\nu]$ is an antisymmetric tensor which represents a field strength, and η is a set of scalar and spinorial fields (which are directly associated with the participating fermions). Each interaction (Electromagnetic, Weak, Strong) contributes a Yang-Mills Lagrangian to the complete Standard Model one. For completion, we list this three Lagrangians in Table 1.1, where one can elucidate some of the properties of the interactions they describe.

[3] These two are actually mixed and so unified, as the QED Lagrangian symmetry group is $U(1)_{em}$, with electric charge Q as its generator.

Symmetry Group	# Generators	Bosons	Field Tensor
$U(1)_Y$	1	B_μ	$B_{\mu\nu} = \partial_\mu B_\nu - \partial_\nu B_\mu$
$SU(2)_L$	3	W^i_μ	$W^i_{\mu\nu} = \partial_\mu W^i_\nu - \partial_\nu W^i_\mu - g\epsilon^{ijk} W^j_\mu W^k_\nu$
$SU(3)_C$	8[4]	G^i_μ	$G^i_{\mu\nu} = \partial_\mu G^i_\nu - \partial_\nu G^i_\mu - g_S f^{ijk} G^j_\mu G^k_\nu$

Table 1.1: Lagrangians for the interactions of the Standard Model. The indices i, j, k, take on the values from 1 to the number of generators for the group, so that there are three W_μ and eight G_μ.

The first striking difference to note is the Lagrangian of $U(1)_Y$ group does not have any self interaction terms, whereas the other ones have. This means that there is no photon-photon interaction vertex, but there exist vertices for gluon and weak boson scatterings.

None of the fields described by the B_μ, W^i_μ directly represent physically observable states. Instead, they are mixed as linear combinations of the physical *mass eigenstates*, which relate to this quantities as:

$$\begin{aligned} W^\pm_\mu &= \frac{1}{\sqrt{2}} \left(W^1_\mu \mp i W^2_\mu \right) \\ A_\mu &= \cos\theta_W B_\mu + \sin\theta_W W^3_\mu \\ Z_\mu &= -\sin\theta_W B_\mu + \cos\theta_W W^3_\mu \end{aligned} \tag{1.2}$$

And by means of this mixing, the electromagnetic and weak coupling constants are related to each other: $\sin\theta_W = g_{em}/\sqrt{g^2_{em} + g^2_W}$. Note however that this transformations should take place *after* electroweak symmetry breaking, because up to this moment all we have been dealing with is a regular Yang-Mills theory, and such theories require the gauge bosons to be massless in order to preserve Lorentz gauge invariance. It is only after the gauge bosons acquire mass while respecting Lorentz invariance through the Higgs mechanism that the mass matrix of this electroweak sector can be built and consequently diagonalized to get the mass eigenstates.

To resolve the part we have not yet dealt with, we first introduce the notation for the classification of particles within the Standard Model in terms of their helicity. Left-handed particles are put into $SU(2)_L$ doublets, and right-handed ones, like [11]:

$$\begin{aligned} \psi^L_j &= \begin{pmatrix} \psi^L_{j+} \\ \psi^L_{j-} \end{pmatrix} \\ \psi^R_j &= \psi^R_{j\sigma} \end{aligned}$$

[4] Actually there are nine generators for $SU(3)$, but one of them, a color siglet gluon, is absent. For a discussion, see [16].

where the $\sigma = \pm$ component index is irrelevant in the right-handed states, as is shown by the equation, precisely because they are singlets. The j is a family index within the range of both quarks and leptons. With this given now, we can complete the Yang-Mills component of the SM Lagrangian, by specifying the η, for the electroweak sector, of Equation 1.1 by:

$$\eta = \sum_j \psi_j^L + \sum_j \psi_j^R \tag{1.3}$$

And the respective covariant derivative D_μ given by:

$$D_\mu = \partial_\mu - ig_W I_a W_\mu^a + ig_{em}\frac{Y}{2}B_\mu + ig_S H(j)\frac{\lambda^a}{2}G_\mu^a \tag{1.4}$$

where I_a is the a component of the weak isospin operator set, and λ^a is the a-th color operator, and $H(j) = 1$ for j indexing quarks, and $H(j) = 0$ otherwise, an artificial factor introduced by us simply to account for the fact that leptons do not experience the strong interaction (as they are color singlets), and so being able to write everything in a little more compact way.

So far so good, but you can easily notice there are no mass terms in this Lagrangian, and simply introducing them "by hand", adding terms quadratic in the fields makes the Lagrangian violate Lorentz gauge invariance[18, 2]. Therefore, a sound method to give rise to the mass terms has to be invoked. It is this method which we discuss now.

1.1.2 The Higgs component

For the SM Lagrangian to remain renormalizable and gauge invariant with the inclusion of mass for the weak bosons, there has to be a symmetry breaking mechanism that renders the $W_\mu^\pm$, Z_μ fields massive, as well as giving mass to the fermions to which they couple by the $SU(2)_L$ interaction. In the minimal model for the SM, the object neeeded to perform such symmetry breaking is a complex $SU(2)$ doublet of the form:

$$\Phi = \begin{pmatrix} \phi^+ \\ \phi^0 \end{pmatrix} = \begin{pmatrix} \phi_1 + i\phi_2 \\ \phi_3 + i\phi_4 \end{pmatrix} \tag{1.5}$$

where the ϕ^i are real scalar fields. Thus this gives the doublet 4 degrees of freedom, adjustable to the requeriments of $SU(2)_L \times U(1)_Y$ symmetry breaking while leaving $U(1)_{em}$ symmetry unbroken. This has, as consequence, the generation of the masses of the weak bosons, keeping the photon massless as it needs to be. The details of the calculations are given in [2]. This conditions renders all but the ϕ_0 component zero, which also acquires a non-zero vacuum expectation value:

$$\langle\Phi\rangle_0 = \langle 0|\Phi|0\rangle = \frac{1}{\sqrt{2}}\begin{pmatrix} 0 \\ v \end{pmatrix} \text{with } v = \left(\frac{1}{\sqrt{2}G_F}\right) \approx 246.211\,\text{GeV} \tag{1.6}$$

Where G_F is the Fermi weak coupling constant. This allows to formulate the field as a perturbation of the vaccum with the introduction of a real scalar function H:

$$\Phi = \frac{1}{\sqrt{2}} \begin{pmatrix} 0 \\ v + H \end{pmatrix} \tag{1.7}$$

The full Higgs Lagrangian results in[11]:

$$\begin{aligned} \mathcal{L}_{\text{Higgs}} =& \frac{1}{2}(\partial^\mu H)^2 - 2\frac{\lambda v^2}{2}H^2 + \frac{\lambda v^4}{4} - \lambda v H^3 - \frac{1}{4}\lambda H^4 \\ &+ \left(\left(\frac{1}{2} g_{em} v \right)^2 W^{\mu +} W^-_\mu + \frac{1}{2} \left(\frac{1}{2} \sqrt{g_{em}^2 + g_W^2}\, v \right)^2 Z^\mu Z_\mu \right) \left(\frac{H^2}{v^2} + 2\frac{H}{v} \right) \\ &- \frac{H}{v} \sum_f \left(\frac{1}{\sqrt{2}} v \lambda_f \right) \bar{\psi}^f \psi^f \end{aligned} \tag{1.8}$$

With the f denoting an index for the fermions. On can directly read the masses of the Higgs, weak bosons and charged fermions:

$$m_H = \sqrt{2\lambda} v \tag{1.9}$$

$$m_W = \frac{1}{2} g_{em} v \tag{1.10}$$

$$m_Z = \frac{1}{2} \sqrt{g_{em}^2 + g_W^2}\, v \tag{1.11}$$

$$m^f = \frac{1}{\sqrt{2}} v \lambda_f \tag{1.12}$$

where the λ_f are several coupling factors, one for each fermion, and λ is, with v, a free parameter arising from the choice of a particular solution of the minimization of the Higgs scalar potential so as to set the vacuum minimum energy point, and in view of the remaining Higgs terms, it can be interpreted as a Higgs self-interaction strength. As we saw on Equation 1.6, we can fix the value of v, but the λ are free in principle, so we have to fix them by experiment. Henceforth the mass of the Higgs particle is a free parameter, and so this is the main motivation for the present work.

1.2 Properties of the Higgs particle

1.2.1 Higgs Mass Constraints

The mass constraints shown in this section come from purely theoretical arguments. A discussion of experimental bounds is found in chapter 2.

Theoretical bounds for the Higgs mass arise by requiring the invariant amplitude of weak boson scattering to be less than one, and from renormalization of the Higgs self-interaction parameter λ. The most stringent among these two limits is the renormalization condition, so this is the one we explore. The renormalization group equation for the Higgs self-interaction λ is[2]:

$$16\pi^2\frac{d\lambda}{dt} = 24\lambda^2 - 3\lambda(g_{em}^2 + 3g_W^2 - 4g_t^2) + \frac{3}{8}(g_{em}^4 + 2g_{em}^2 g_W^2 + 3g_W^4) - 6g_t^4 + \cdots \quad (1.13)$$

with $t = \ln(Q^2/v^2)$ a normalized (with respect to the vacuum expectation value v) energy scale and $\lambda_t = m_t/v$ the Higgs-Top quark coupling constant. As a differential equation, its solutions will be sensitive to the initial value $\lambda(t=0)$. The relevant fact is that the Higgs self-interaction has to remain finite for all the energy scales in which the Standard Model is supposed to be valid (We know it has to break down at some energy, due to the shortcomings we discussed before). For large positive λ, there should be no Landau pole for energies below a cutoff scale Λ. In this situation, the first term dominates the series and the solution to the equation is:

$$\lambda(Q) \approx \frac{\lambda}{1 - \frac{3}{2\pi^2}\lambda\ln(t)} \quad (1.14)$$

Which shows a Landau pole at:

$$Q_{\text{Landau}} \approx v\exp\left(\frac{4\pi^2 v^2}{3m_H^2}\right) \quad (1.15)$$

We present Landau poles for some values of the Higgs mass in Table 1.2. Note how rapidly it decreases with increasing Higgs mass, being very close to the Higgs mass when this is around 800 $\mathrm{GeV/c^2}$. This sets an upper bound to the Higgs mass, and as we anticipated earlier, the scenario of a Higgs decay width greater than the Higgs mass cannot take place, for if the Higgs mass happens to be greater than the 1 TeV level, new physics have to come into play. Instead, if the Standard Model is to be valid up to the Planck scale (around 10^{19} GeV), we see from the Table 1.2 that m_H should be less than about 140 $\mathrm{GeV/c^2}$. The arguments just presented are the so called Triviality arguments. To obtain a constraint from below, first recall that λ cannot be negative, as there would not be an energy minimum at the vacuum expectation value. That is, there would be no stable minima. What follows is called the Stability argument[2]. So for small positive $lambda$, the Higgs-Top quark coupling dominates, and a similar procedure as the previous one follows, with the renormalitzation group equation for the Higgs-Top quark coupling in the limit of low m_H being solved with a funcion of similar form as in Equation 1.15 (for the details, see [2]), yielding a theoretical lower bound of 3.7 $\mathrm{GeV/c^2}$for the Higgs mass.

1.2.2 Higgs Decay Modes

From the expressions above, looking at the terms which are linear in the Higgs field H, one can notice that the Higgs couplings to the fermions are linear in the fermion masses,

m_H (GeV)	Q_{Landau} (GeV)
80	$3.340 \cdot 10^{56}$
100	$1.086 \cdot 10^{37}$
200	$1.128 \cdot 10^{11}$
400	$3.602 \cdot 10^{04}$
800	856.31

Table 1.2: Landau poles for several Higgs masses, calculated with Equation 1.15.

whereas the couplings to the weak bosons are quadratic in the boson masses. This naturally affects the decay widths for the Higgs branching into each of these particle species. In equations (1.16) and (1.17), where the Higgs decay widths to fermions and bosons respectively are given, we will confirm these appreciations:

$$\Gamma(H \to f\bar{f}) = \frac{N_C g_{em}^2 m_f^2}{32\pi m_W^2} \left(1 - x_f^2\right) m_H \tag{1.16}$$

$$\Gamma(H \to V\bar{V}) = f_V \frac{g_{em}^2}{128\pi} \frac{m_H^3}{m_W^2} \left(1 - x_V^2\right) \left(1 - x_V - \frac{3}{4} x_V^2\right) \tag{1.17}$$

with $x_o = 2\frac{m_o}{m_H}$, $f_V = 1$ for the case $V = Z$ and $f_V = 2$ for $V = W$, and N_C a color factor which is 3 for f tagging quarks, and 1 for leptons. Here we note the strong cubic dependence of the bosonic decay width on the Higgs mass, contrasting the linear dependence of the fermionic decay width. It is therefore easy to guess that as soon as phase space allows, the bosonic decay modes will quickly become the dominant decay modes, so they are the most viable channels for Higgs search endeavors. In Figure 1.1 we show the different decay channels of the Higgs, and how they evolve as the Higgs mass varies. Note that, as it can be learned from the SM Higgs Lagrangian component, the Higgs does not couple to photons and gluons, and so decay modes involving these massless bosons proceed through (heavy) fermion loops. Note also that the functional forms of the decay widths find a point in which they add up to a number higher than the very same Higgs mass (which happens at about $m_H = 1.4\ \text{TeV/c}^2$). This poses a problem in interpreting the Higgs field excitations as particles, and so we may set an upper bound for the Higgs mass. However, since by now the Higgs boson mass is constrained to be a few hundred GeV/c^2, it is unlikely that this case shows up in the experiment. In Figure 1.2 we reproduce a calculation of the total decay width, to complete the picture of the present discussion.

1.2.3 A remark in the Higgs production cross section

The main production modes for Higgs boson production are gluon fusion and vector boson fusion, of which the gluon fusion mode dominates. Their Feynman diagrams are shown in Figure 4.1. Also associated production or *Higgstrahlung* modes

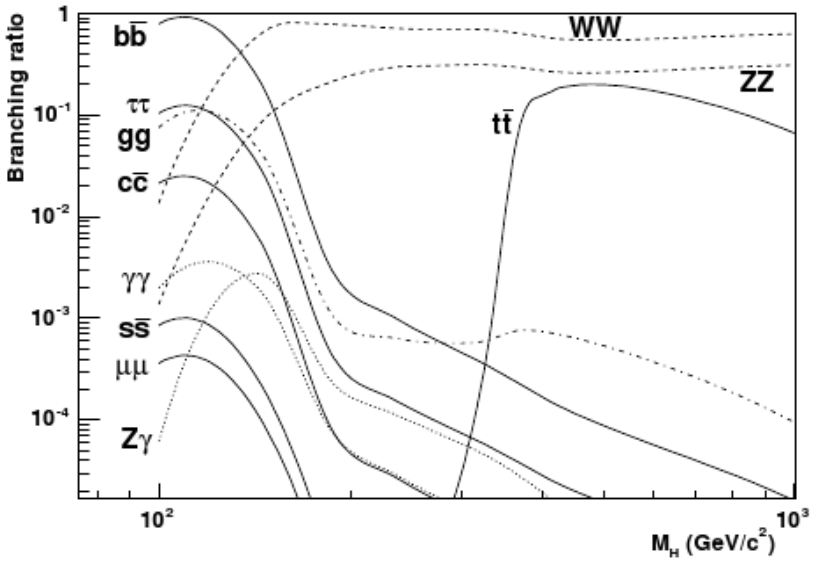

Figure 1.1: Evolution with Higgs mass of the different decay modes. Taken from [10].

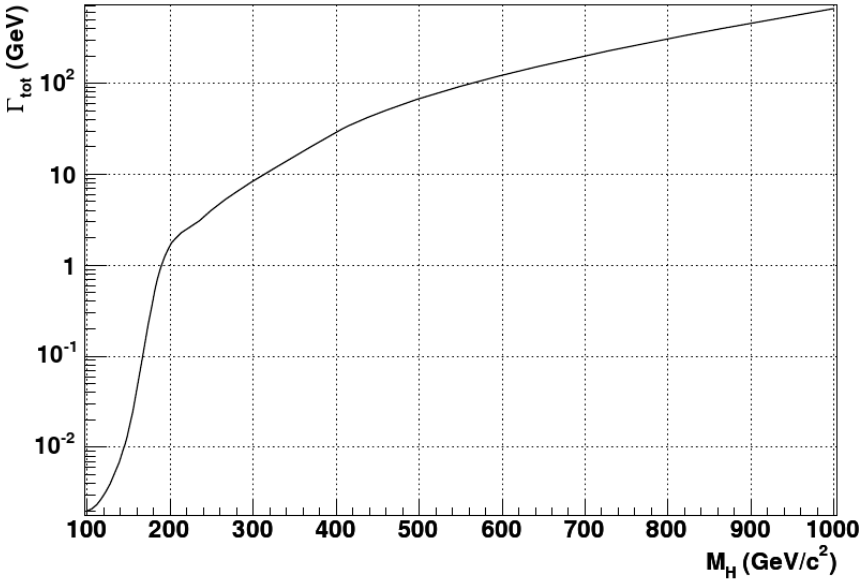

Figure 1.2: Evolution with Higgs mass of the total decay width. Taken from [10].

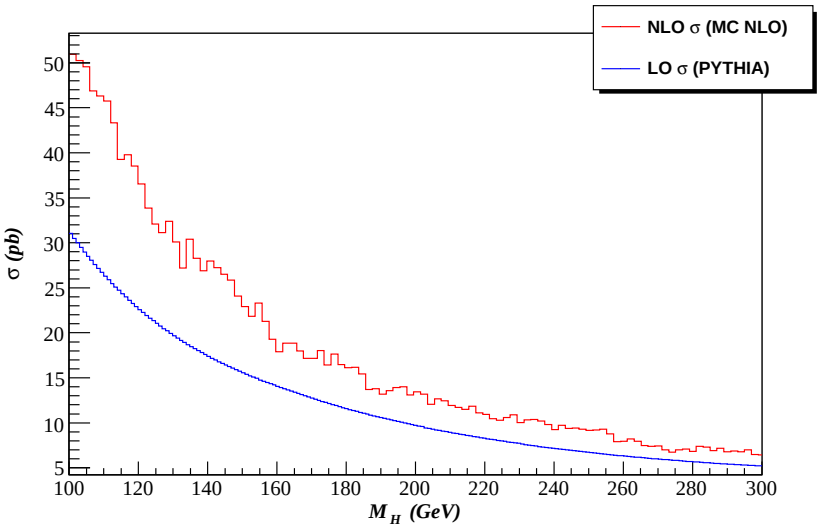

Figure 1.3: Comparison between NLO and LO production cross sections for the LHC scenario. The NLO data was generated with the MC@NLO code, and the LO data with PYTHIA.

are present, but their total cross section is smaller than the modes we consider here. The gluon fusion cross section is strongly affected by Next-to-Leading Order (NLO) QCD corrections[23], arising from the large Higgs-Top quark coupling strength. The relevant Feynman diagrams are shown in Figure 1.4. The effect is noticeably non negligible, and so NLO calculations of Higgs processes need to be performed whenever possible. In this study we simulate all Higgs processes at NLO, so as to get more up-to-date results. Note the cross section correction factor can grow up near 2.

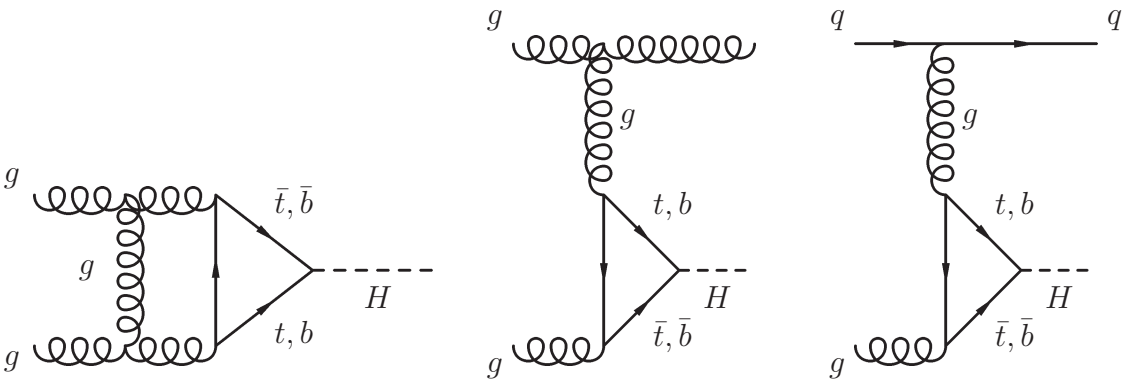

Figure 1.4: Feynman diagrams for QCD corrections to the Higgs production cross sections

Chapter 2

Experimental Higgs searches

In the following we summarize experimental results for several Higgs searches done at CERN and Fermilab, and discuss the implications they have on the prospect for a Standard Model Higgs boson discovery. Higgses from other models, like those which extend the Standard Model with Supersymmetry, are not discussed.

2.1 Searches at CERN

Part of the data analises of the experiments at the LEP accelerator were dedicated to search of the Higgs boson. The experiment ran from 1989 until 2000, where it was shut off. Its center of mass energy was initially 46 GeV, and by the end of its lifetime it had scalated to 209 GeV. Thus, for the purpose of Higgs searches, it was only tailored for light Higgs masses. Since it is an electron-positron collider, the accelerating particles suffer from large bremstrahlung effects, and so increasing the beam center-of-mass energy is very costly, and making it better to use heavier particles to achieve higher energies. On the other hand, lepton collisions offer the cleanest conditions for scrutinies in the electroweak sector, as low QCD backgrounds are produced.

Since electron-positron collisions give rise to intermediate boson states (among which Higgs could also be present, but as we saw earlier, its coupling to leptons is as low as their mass, and so this events prove highly unlikely), the dominant Higgs production mode at LEP is the Higgstrahlung mechanism, whose corresponding Feynman diagram we show in Figure 2.1. For low energies, like those used in the LEP1 era (46 GeV CM energy), the final Z boson is produced off-shell, whereas above threshold, it is on-shell. In view of Figure 1.1, for the kinematically accesible range of Higgs masses for the LEP, the dominant decay mode for the Higgs boson is a pair b -$\bar{b}$ quark pair, or even, not so often though, τ^+ τ^- pairs. So the final picture most likely contains two b-jets and two leptons, another pair of jets or missing transverse energy. The most important result from the LEP results and analises is the lower bound established by a likelihood ratio method[10], to test the results against several Higgs mass hypothesis. A test statistic $-2\ln Q$ was built, with the purpose of comparing the data with

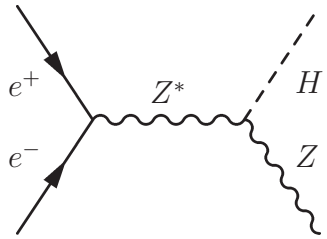

Figure 2.1: Feynman diagram for Higgstrahlung mechanism.

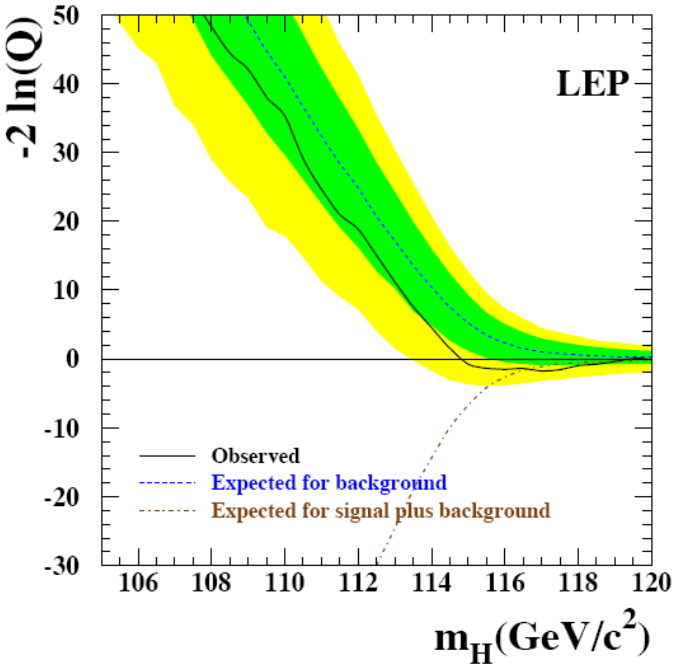

Figure 2.2: Test statistic for LEP data. Taken from [17].

background-only (the Higgs particle does not exist) and signal+background (the Higgs particle exists and its events are scattered along with the backgrounds) hypothesis, generated by several Monte Carlo experiments. The results are presented in Figure 2.2. The data used for the present construction was gathered when the LEP was working at energies varying from 189 GeV up to 209 GeV. Note the excess of events in the experimental data for Higgs masses greater than 114 $\mathrm{GeV/c^2}$. By now it is established that it represents a variation of 1.7 standard deviations[17]. The observed lower bound for the Standard Model Higgs mass was then calculated at the 95% confidence level to be 114.4 $\mathrm{GeV/c^2}$.

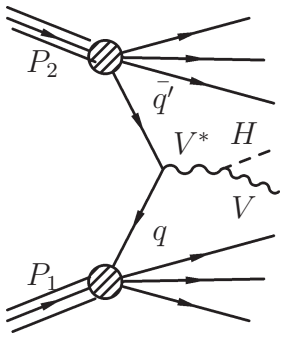

Figure 2.3: Feynman diagram for associated Higgs production.

2.2 Searches at Fermilab

The D∅and CDF experiments at Fermilab both have dedicated Higgs search groups, which are currently processing and analyzing the data originating from the $p\bar{p}$ collisions at a center-of-mass energy of 1.96 TeV. The multijet output of the collisions make the analises favor the leptonic final states of the associated Higgs production process, whose Feynman diagram we depict in Figure 2.3. At present, the two collaborations have set upper bounds on the cross sections for the associated production channel as well as the Higgs-alone channel. Those results are shown in Figure 2.4. Projections for when 8 fb^{-1} of integrated luminosity had been gathered indicate the data will be able to exclude(discover) at the 95% confidence (with significance higher than 3σ) a Higgs boson with a mass range of 115 $\mathrm{GeV/c^2}$up to 185 $\mathrm{GeV/c^2}$[3]. Also, the published D∅results for 1 fb^{-1} of integrated luminosity have excluded a fourth generation of fermions if the Higgs has a mass in between 150 $\mathrm{GeV/c^2}$and 185 $\mathrm{GeV/c^2}$. This is because fourth-generation fermions, being heavier than the very top and bottom quarks, would have an appreciable effect increasing the production cross section of the Higgs (recall that the Higgs-particle coupling strength grows at least as the mass of the particle). For the $H \rightarrow WW$ channel, the studies at both experiments employ, before applying discriminant techniques (like likelihood tests, neural networks, etc.), kinematic cuts on the events. These kinematic cuts can be categorized as detector-related and dynamics-related. Detector-related cuts have to do with trying to minimize the impact on the final data of detector effects like lepton misidentification, cosmic-ray dummy events, to list some. Dynamics-related cuts are the ones that actually deal, after correcting for detector effects, with the underlying differences in the distributions of the kinematic variables of the signals and the backgrounds. The kinematic cuts listed on Table 2.1 are to be contrasted with the ones we apply to our generated data, listed on Table 4.4. These are taken from several CDF and D∅reports([6, 5]). The similarity with the cuts applied in our study is clear. However, we attemp to exploit the angular distributions affected by the spin correlations of the Higgs decays.

The aforementioned dependence of the fermion masses on the fermion-Higgs cou-

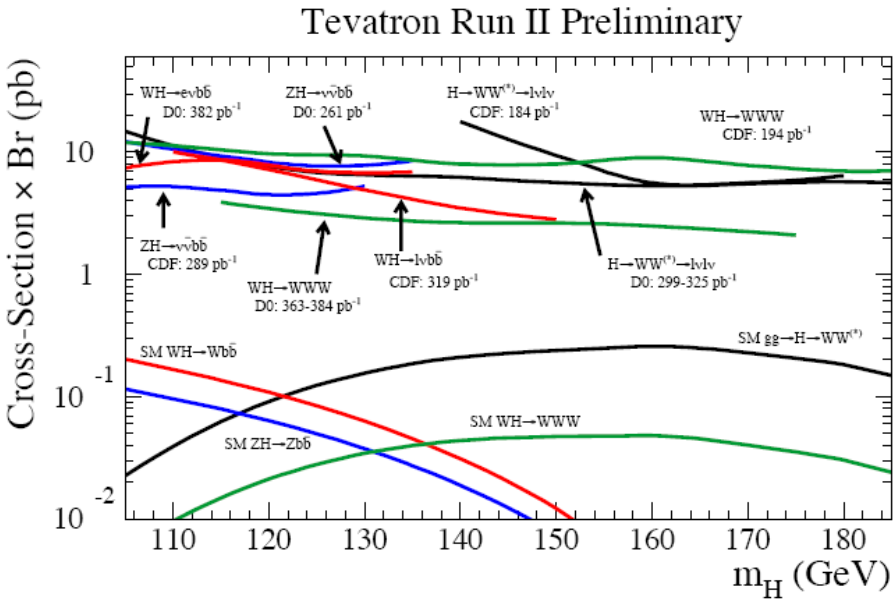

Figure 2.4: Cross section upper bound from CDF and D∅. The curves at the bottom are the Standard Model predictions. Taken from [17].

pling strength (as well as the weak boson-Higgs coupling strength) provides a method for estimating the unknown Higgs mass through precision measurements of the masses to which the Higgs couples strongest, like the W, Z bosons and the top quark. In figures 2.5, 2.7 and 2.6 several studies for a range of Higgs mass hypothesis are shown, carried by the LEP Electroweak Working Group. From the figures one can infer, as it is also stated on related articles[20], that the electroweak predictions favor a light Higgs. For instance, review Figure 2.6. The region enclosed by the 68% CL contour does not extend further in Higgs mass than 200 $\mathrm{GeV/c^2}$. The constraint from the top quark mass is not so stringent, but at any rate, the last one is just another reason for the Standard Model to favor a light-intermediate Higgs mass in case the Higgs boson exists.

Finally, Figure 2.8 shows the sensitivity per experiment at the Tevatron for Higgs signals. The picture indicates the Tevatron only has a chance for Higgs exclusion if its mass is less than about 185 $\mathrm{GeV/c^2}$, and for evidence, the Higgs needs to be lighter than 130 $\mathrm{GeV/c^2}$for the Tevatron to give an evidence before it undergoes shutdown. For a discovery, the Higgs would need to be lighter than the present lower bound, and so the Tevatron is not likely to provide any practical discovery statistics.

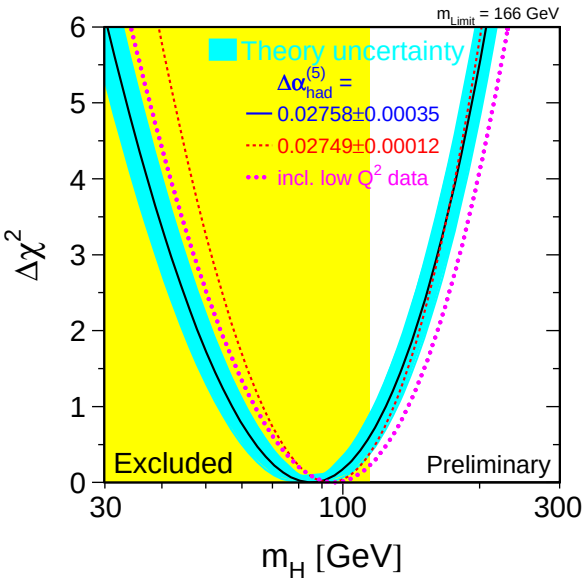

Figure 2.5: Goodness-of-fit evolution for the data as it changes with the Higgs mass hypothesis. The blue band is an estimated theoretical error due to higher-order corrections not taken into account. The yellow region corresponds to the exclusion set by the LEP studies (95% CL exclusion). Taken from [7].

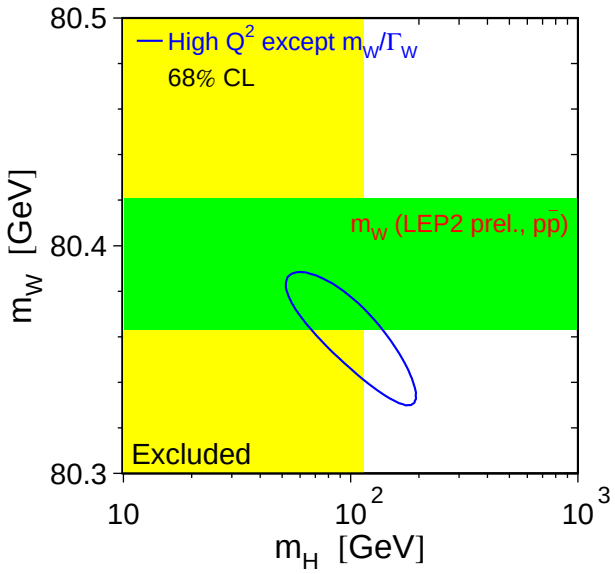

Figure 2.6: W-Higgs mass correlations through radiative corrections. The blue contour corresponds to the 68% confidence level. The green band is the scattering region within $\pm 1\sigma$ for the direct measurements data. The yellow band is the excluded region, established by the LEP studies (95% CL exclusion). Taken from [7].

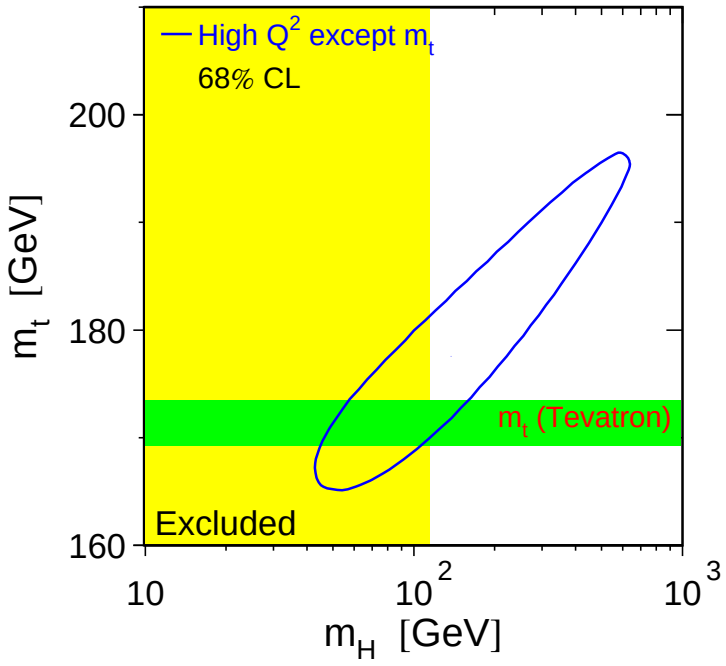

Figure 2.7: Top-Higgs mass correlations through radiative corrections. The blue contour corresponds to the 68% confidence level. The green band is the scattering region within $\pm 1\sigma$ for the direct measurements data. The yellow band is the excluded region, established by the LEP studies (95% CL exclusion). Taken from [7].

Cut Specification	Value (GeV)
Transverse Momentum	$p_T^{\ell\text{lead}} > 20$ and $p_T^{\ell\text{trail}} > 10$ ($M_H = 120\text{GeV/c}^2$)
	$p_T^{\ell\text{lead}} > 20$ and $p_T^{\ell\text{trail}} > 10$ ($M_H = 120\text{GeV/c}^2$)
	$p_T^{\ell\text{lead}} > 20$ and $p_T^{\ell\text{trail}} > 15$ ($M_H = 140\text{GeV/c}^2$)
	$p_T^{\ell\text{lead}} > 25$ and $p_T^{\ell\text{trail}} > 15$ ($M_H = 160\text{GeV/c}^2$)
	$p_T^{\ell\text{lead}} > 25$ and $p_T^{\ell\text{trail}} > 15$ ($M_H = 180\text{GeV/c}^2$)
Missing Transverse Energy	$25 < \not{E}_T < 70$ ($M_H = 120\text{GeV/c}^2$)
	$25 < \not{E}_T < 80$ ($M_H = 140\text{GeV/c}^2$)
	$30 < \not{E}_T < 90$ ($M_H = 160\text{GeV/c}^2$)
	$35 < \not{E}_T < 100$ ($M_H = 180\text{GeV/c}^2$)
	$35 < \not{E}_T < 110$ ($M_H = 200\text{GeV/c}^2$)

Table 2.1: Kinematic cuts by Higgs mass ranges at D∅(from [6]). The cuts listed on [5] were similar, and so are not explicitly included here.

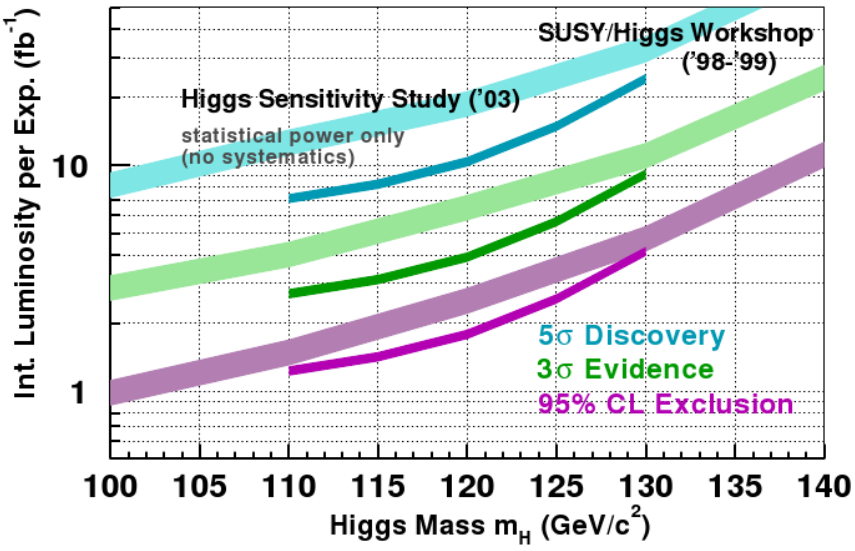

Figure 2.8: Tevatron sensitivity of CDF/D∅combined experiments for the SM Higgs signal. The narrow lines show the results from the most recent study, done in 2003. Taken from [4].

Chapter 3

Computational Setup

The development of this thesis has been done with the help of several programs, which we list in Table 3.1.

Program	Reference	Version	Purpose
PYTHIA	[22]	6.4.12	Multipurpose event generator with showering and hadronization
HERWIG	[8, 19]	6.5.10	Multipurpose event generator with showering and hadronization
MC@NLO	[12, 13]	3.3	NLO matrix element generator with parton shower matching
ROOT	[1]	5.17/05	High-Energy Physics inspired data analysis framework

Table 3.1: List of programs used in this thesis.

3.1 PYTHIA and HERWIG

These two programs are FORTRAN Monte Carlo codes intended to provide a platform for High Energy Physics event generation and analysis. They implement a variety of physics processes, with emphasis in QCD interactions, and so they are suited for physics events generation, which for a full statistical study would then undergo a detector simulation phase, after which the data are directly comparable with the experimental data, in order to test/validate physical hypothesis. They are specially suited for hadron-hadron collisions (Nowadays this means, in practice, proton-(anti)proton collisions), which, apart from the basic parton-level interactions, present several complexities like initial and final state radiation with multiple interactions, along with the hadronization of the products of the simulated parton-level processes. For a better illustration on the elements of Monte Carlo event generators, see [21]. These programs are closely related

to each other in purpose, but their implementations of the physics processes are completely independent. For instance, the hadronization out of quarks and gluons is done by PYTHIA invoking the *String Fragmentation* model, whereas HERWIG follows suit by use of the *Cluster Model*. The first picture, qualitatively, describes the splitting of partons by the eventual breaking of color strings joining them, as (due to the presumably linear form of the strong force potential) the potential energy contained in their joining string grows with their separation. The second picture exploits the preconfinement property of QCD to form color-neutral clusters of quarks or diquarks which then decay into the final hadrons.

The use of these codes is also very similar. They are to be used almost like libraries in an usual FORTRAN program, which has the role of parameter configurator and data logger/analyzer. The user program sets some function switches related to its workings and to the physics processes to be simulated, and usually sets up an event loop, where there is one(in the case of PYTHIA) or several (in the case of HERWIG) routines that need to be called in order to generate a collision, perform the parton-level hard processes, and if required, generate the hadronization, multiple interactions, initial and final state radiations and underlying events (these are the ones involving spectator partons). Only one collision is simulated per loop iteration, in contrast with physical events inside a collider, where bunches of incident particles collide. Next the user program usually needs to do some data logging of the results calculated by the event generator code, and most likely some analysis routines too, after which the user may choose to print the results and/or save them to disk.

The idea behind the use of goal-like programs however, beyond the sake of comparison, is because the third program, MC@NLO, uses HERWIG as its showering and hadronization machinery, which is what we now discuss.

3.2 MC@NLO

As it has been discussed in chapter 1, the importance of QCD corrections to the processes we study in this work should not be ignored if one is attempting to provide reasonable statistical estimates. This corrections constitute next-to-leading order contributions to the original matrix elements, which because by several technical and theoretical reasons (which are addressed in the program references given in the Table 3.1) cannot be directly added to the Leading-Order code in the event generators. A solution to that problem is the program we are dealing with now. The overall execution of this code takes place in two phases. In the first one, the program generates parton-level events with NLO corrections included (this phase usually takes as much or more time than the execution of the conventional event generator). The result from this execution is a set of files which are then read by the second phase program, which is nothing more than a standard HERWIG user program with some interface routines provided by

the package, all this enabling the user to obtain NLO-corrected events and treat them identically as HERWIG-generated events.

The mode of utilization is not so different to that of a normal event generator. The user will need to change a formatted input file with the parameter selections relevant to her/his purposes, that will configure the run of a first phase of the program and part of the second phase. Also the user has to supply the previouly mentioned user program, more specifically, the initalization, analysis and ending routines, as the structure of the body of the program should not be changed to avoid complications.

Besides NLO contributions, the program also accounts for the spin correlations in most of its implemented processes, and this a very important feature, as precisely these spin correlations are one of the most useful criteria in the discrimination of signal and background events in the present study. At any rate, fortunately both HERWIG and PYTHIA themselves include spin correlations for the processes we want to simulate.

3.3 ROOT

ROOT is a data analysis framework developed at CERN (and so inspired in the activities of High Energy Physics). It features a rich set of tools for data acquisition, storage, processing (all these options with the facility of distributed or parallel execution), analysis and publishing, implemented as C++ libraries, against which user programs can be coded and compiled for stand-alone execution, and also the possibility to use them interactively through a C++ interpreter, CINT[15], which allows for rapid prototyping of user-defined functions, and thus gives ROOT an enormous flexibility.

Among the manifold of characteristics ROOT provides, of special interest is the Artificial Neural Network facility implemented in the *TMultiLayerPerceptron* class[9]. It implements a multilayer perceptron which takes its training and test sets from a TTree class (which is a data storage structure, completely configurable by the user). It presents several training methods which the user can choose and tweak to some extent, and several functions (including those within the *TMLPAnalyzer* class) to observe and quantify the behavior of the network after training. The versatility of neural networks includes operation as universal continuous function approximators (this means, they provide an alternative to traditional data-fitting methods) as well as classificators (which is the use we employ in this study). Let us briefly introduce this facility.

The Multilayer Perceptron type of Neural Networks (there are many others) consists of a set of asynchronous parallel processing units (called neurons), connected to each other through *synapses* (which are weighting connections), and whose outputs are evaluations of a linear combination of their inputs (the weigths of the linear combination are set by the synapses) with a special function. However, for the neurons of

the input and output layers, the special function is at most a normalization/rescaling. An example of a structure for a multilayer perceptron is depicted in Figure 3.1. This figure is automatically generated by the *TMultiLayerPerceptron* class after being configured for its inputs, number of neurons per hidden layer (these layers are the ones in between the input and output layers), type of function for the neurons of the hidden layers, and normalization options. The thickness of a connecting line (the synapses we mentioned before) is proportional to the magnitude of the weight of that synapse. The most common special function of a hidden-layer neuron is a sigmoid (or logistic) function, defined as $1/(1+e^{-x})$, although there are several other options included in the class. The fundamental idea is to construct an universal function approximator (Because it has been proved that a linear combination of sigmoid functions can approximate any continuous function) through some ”training” procedure, by which the weigths of the network are configured in order to program the network with a desired behavior as a function of the inputs. More formally, one is to perform an iterative procedure (whose steps are called ”epochs” in the class) by which an error function of the obtained/specified outputs are compared, in order to have this error function tend as close to zero as possible. The class implements several training methods with a few parameters to be tuned by the user as needed. When the class is set into training mode, among the options available is the one to show an evolution of the error of the network as the training iterations are performed. An example of a (not so succesful) training exercise is shown in Figure 3.2. In the training, a set of data is used to perform the error-minimization procedures, and also another *test* set is used for comparison. As inputs the class requires a string dictating the layout of the network, a *TTree* data container object out of which the training/test data sets will be built, and a specification for the construction of such training and test data sets.

After the training is done, the class implements functions for evaluating the performance of the network. for this short introduction, we chose to show the one that displays a plot of the response of the network, as it is best suited for this classification task. This is illustrated in Figure 3.3. The results shown clearly show a poor performance, as the inputs for background cases result in common output values with a non-negligible set of signal-case inputs. However, it is worth for the illustration. As we said, there are also many more options available for exploration and even *random-play*, but for now the basics have been set.

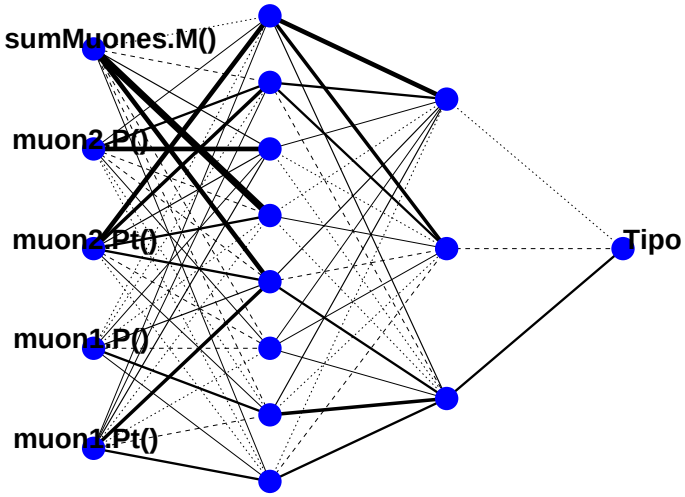

Figure 3.1: Sample of the layout of a multilayer perceptron Neural Network, as it is generated by the *TMultilayerPerceptron* class.

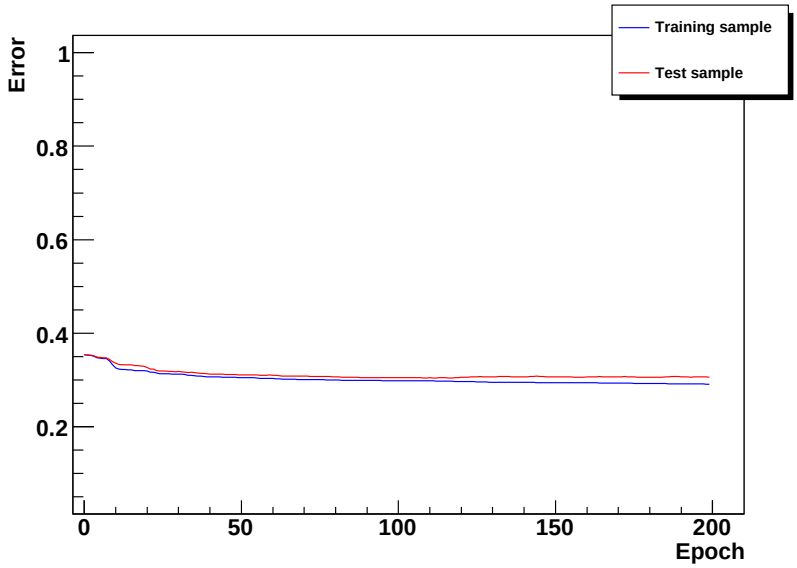

Figure 3.2: Sample training evolution from a *TMultilayerPerceptron*, for a 200 training iterations

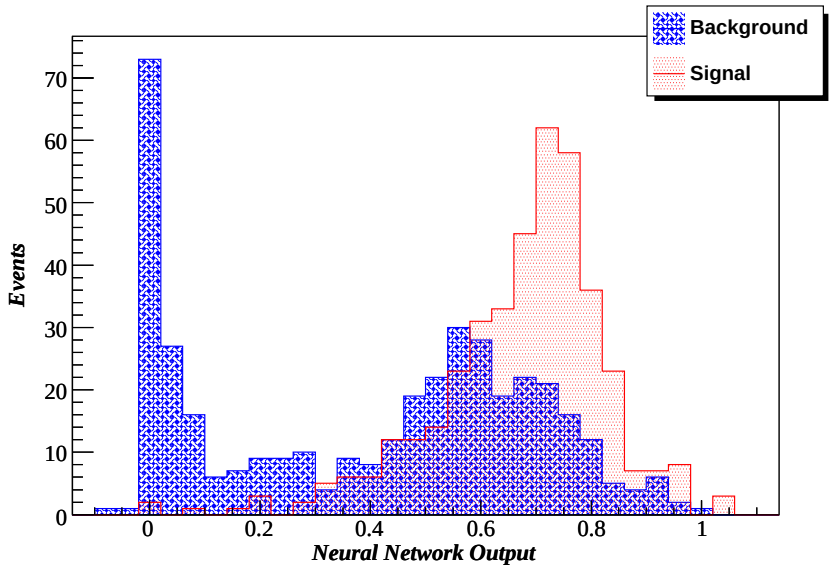

Figure 3.3: Sample output from a *TMultilayerPerceptron* in classification mode.

Chapter 4

Results and Analysis

In the following we detail the results from our simulations and analises . For the signal events, we simulate production of the Higgs boson that branches to a pair of weak bosons $W^{\pm}$ or Z^0, which in turn decay, each of them, to muonic final states. The simulated scenario is that of the LHC, that is, proton-proton collisions with a center-of-mass energy of 14 TeV.

4.1 Physical processes

The process to study is the production of the Standard Model Higgs boson, predominantly through gluon fusion, as well as the smaller contributions from quark anihilation and vector boson fusion. We study the Higgs through its decay modes into pairs of weak bosons, $H \rightarrow Z^0Z^0, W^+W^-$, which we analyze by considering their muonic final states, $Z^0 \rightarrow \mu^+\mu^-$, $W^{\pm} \rightarrow \mu^{\pm}\nu_{\mu}(\bar{\nu_{\mu}})$. The Higgs mass range of values considered, starts from 120 $\mathrm{GeV/c^2}$up to 300 $\mathrm{GeV/c^2}$. Background processes that sever the Signal-to-Noise ratio are listed in Table 4.1. Their kinematical distributions and cross sections are found to be essentially independent of the assumed Higgs mass, in both the LO and NLO calculations.

Signal Event	Background processes
$H \rightarrow Z^0Z^0$	$f\bar{f} \rightarrow Z^0Z^0$
$H \rightarrow W^+W^-$	$gg, q\bar{q} \rightarrow W^+W^-$, $gg \rightarrow t\bar{t} \rightarrow bW^+\bar{b}W^-$

Table 4.1: Listing of the studied physical processes

In order to distinguish signal events among the whole set of generated events, kinematic cuts were established and applied, and the resulting data sets were processed (one for each evaluated Higgs mass) by an Artificial Neural Network, in an intent to achieve

a stronger signal discrimination.

4.2 Production Parameters

For this study, an integrated luminosity of 10fb^{-1} data is projected (This means, this study may be compared with the data gathered at the LHC in the first few months). This dictates the precise number of events to simulate, by knowing the value of the total cross section of each process. The value of these cross sections changes from process to process, and depending on the particular one, it may vary considerably with the order at which it is calculated (as an illustration, check Figure 1.3). In the Table 4.2 we present the production cross sections for the background processes, and in (4.3) they are given for the signal processes, times the corresponding branching ratios, and the resulting number of events to generate. This number of events is taken from the cross sections calculated at NLO.

Process	$\sigma^{\text{LO}} \times \text{BR}$ (pb)	$\sigma^{\text{NLO}} \times \text{BR}$ (pb)	Events @ 10fb^{-1}
$f\bar{f} \to Z^0 Z^0 \to 4\mu$	$1.75 \cdot 10^{-2}$	$1.79 \cdot 10^{-2}$	180
$gg, q\bar{q} \to W^+W^- \to 2\mu\, 2\nu_\mu$	0.825	1.305	13050
$gg, q\bar{q} \to t\bar{t} \to bW^+\bar{b}W^- \to 2\mu\, 2\nu_\mu$ + 2 jets	5.743	6.667	66070

Table 4.2: Production cross sections by process - Background processes

As it is noticeable from the tables, the cross sections for background processes are not strongly affected by the NLO corrections, whereas for the signal processes they are increased by k-factors ranging from 1.2 up to 1.7, which are independent of the branching processes, depending instead of the Higgs production interactions.

4.3 Kinematic cut-based discrimination

The initial signal-to-noise ratio (which from now on we will denote as SNR) is really poor, of the order of 10^{-4}. In this study, only kinematic variables of the detected leptons were considered, with no study of the accompanying jets. As a way to make up for this, the data remaining from the filtering of kinematic cuts were evaluated by an artificial neural network, taking advantage of the capabilities these objects have to exploit hidden, non-linear relations among the presented variables, to have a sharper discriminating power.

Process	m_H (GeV/c^2)	$\sigma^{\mathrm{NLO}} \times \mathrm{BR}$ (pb)	$k-\mathrm{Factor} = \sigma^{\mathrm{NLO}}/\sigma^{\mathrm{LO}}$	Events @ $10\mathrm{fb}^{-1}$
$H \to Z^0 Z^0 \to 4\mu$	100	$7.469 \cdot 10^{-5}$	1.639733	0
	120	$7.462 \cdot 10^{-4}$	1.618308	7
	140	$2.068 \cdot 10^{-3}$	1.610348	23
	160	$8.251 \cdot 10^{-4}$	1.272836	8
	180	$8.848 \cdot 10^{-4}$	1.392206	11
	200	$3.727 \cdot 10^{-3}$	1.380172	39
	220	$3.445 \cdot 10^{-3}$	1.316819	34
	240	$3.077 \cdot 10^{-3}$	1.288302	30
	260	$2.700 \cdot 10^{-3}$	1.257356	27
	280	$2.349 \cdot 10^{-3}$	1.200915	23
	300	$2.252 \cdot 10^{-3}$	1.240482	22
$H \to W^+W^- \to 2\mu\, 2\nu_\mu$	100	$7.316 \cdot 10^{-3}$	1.639733	12
	120	0.0289	1.618308	670
	140	0.1718	1.610348	1718
	160	0.1919	1.272836	1919
	180	0.1750	1.392206	1750
	200	0.1161	1.380172	1161
	220	0.0917	1.316819	917
	240	0.0706	1.288302	760
	260	0.0651	1.257356	651
	280	0.0556	1.200915	556
	300	0.0521	1.240482	521

Table 4.3: Production cross sections by process - Signal processes

It is also important to clarify these data include no detector simulation, so that our results would have to be fed into a detector simulation program like GEANT. This is inevitably going to reduce the available statistics (as detector identification efficiencies are never unity), and the overall effect is to increase the uncertainties in the observables we measure. This also means that the selected kinematic cuts have a direct correspondence with the fundamental dynamics of the processes here involved, and as such are also useful to highlight features of each of them.

4.3.1 The channel $H \to W^+W^- \to 2\mu\, 2\nu_\mu$

As it is apparent from the tables (4.3), (4.2), the present channel has high statistics for the chosen integrated luminosity. Under this circumstance, it is not practical to feed and train the neural network with the raw data, as the multiple training iterations

would make the process impractical. Henceforth it is better first to apply cuts in order to enhance the SNR while reducing the number of background events as much as possible. We now list the set of kinematic cuts effected on the event set:

1. $12 < M_{\mu\mu} < 80$
2. $30 < p_T^{\ell \max} < 55$
3. $40 < \not{E}_T < 80$
4. $\sin(\phi_{\mu\mu}/2) < 0.4$

These criteria mainly arise from the strong spin correlations between the pair of vector boson resulting from the Higgs decay, due to conservation of total angular momentum, as the Higgs is a scalar particle (spin 0) and the bosons are vectors (spin 1). This correlation in turn is transmitted to the final detected leptons. This fact constitutes in principle a sensible difference in the angular distributions of the detected leptons, as the vector bosons from the Higgs are produced in the s channel, whereas the ones originating from background processes are created in the t channel. See the Feynman diagrams for these processes in Figure 4.1. In the Figure 4.4 the distribution of the angular separation of the detected muons is shown for the background processes, noticing the trend for these to be diametrically opposed to each other. For comparison, the figures 4.2 and 4.3 (which qualitatively agree for a lower part of the Higgs mass range, and then the PYTHIA results favor a rather isotropic distribution) show the behavior of the latter distribution for the signal events, as the Higgs mass runs within the interest range, for each 20 $\mathrm{GeV/c^2}$. It is interesting to notice that the distribution behaves, for Higgs mass values less than 180 $\mathrm{GeV/c^2}$, antagonically with respect to the background distribution. This is of great help in discriminating the events. However, for greater Higgs masses and up to the end of our interest range, the angular distribution becomes, as the Higgs mass grows larger, more alike to the backgrounds one in the MC@NLO results, and isotropic-like in the PYTHIA case, which at any rate makes this channel a difficult one for finding the Higgs if its mass happens to lie in this high mass interval.

It is also worth annotating that to optimize the SNR at each Higgs mass point, the kinematic cuts have to vary in order to account for the relevant kinematic properties of each particular setting. Such search was performed, and it was found that the variations were rather small (a few percent), and furthermore, the kinematic cuts could be applied to subranges of the Higgs mass range. The applied kinematic cuts, categorized this how, are shown in Table 4.4.

It was also observed that this channel is not significative for discovery of a Higgs boson with a mass greater than 200 $\mathrm{GeV/c^2}$, reason by which no kinematic cuts were evaluated for this region of parameter space. The reasons why are not only the angular separation distributions are very alike to the background processes distribution, but also

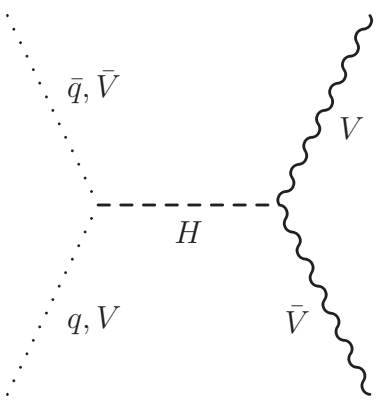

(a) Higgs boson decay in a weak boson pair

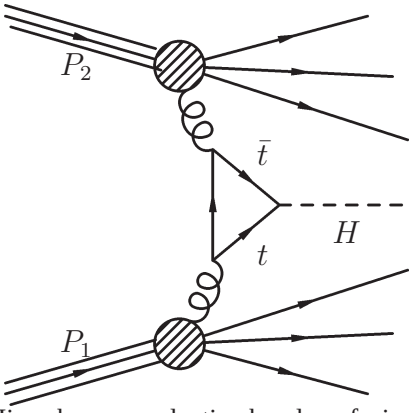

(b) Higgs boson production by gluon fusion

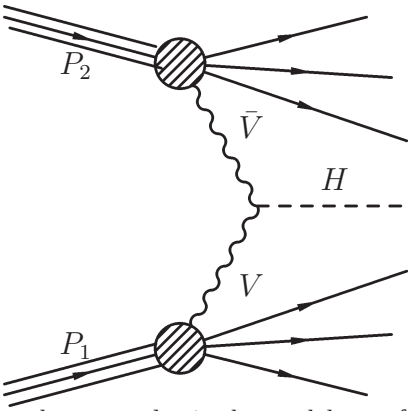

(c) Higgs boson production by weak boson fusion

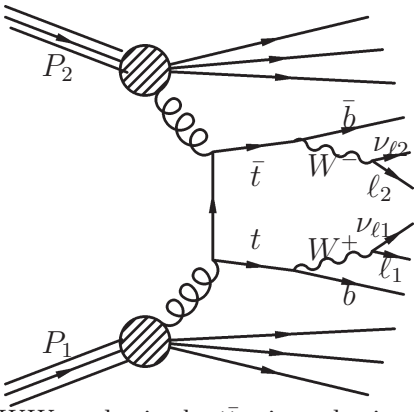

(d) WW production by $t\bar{t}$ pair production

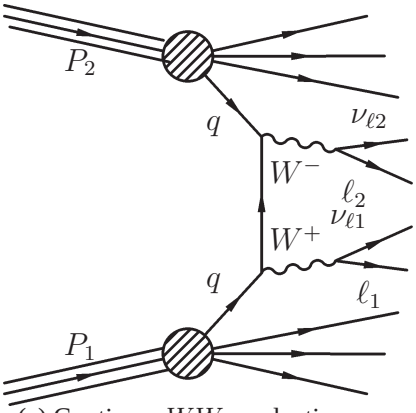

(e) Continum WW production

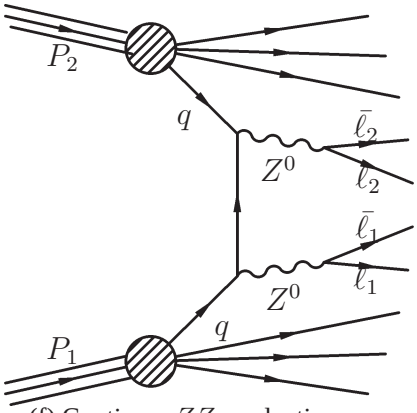

(f) Continum ZZ production

Figure 4.1: Feynman diagrams for the physical processes involved in this study

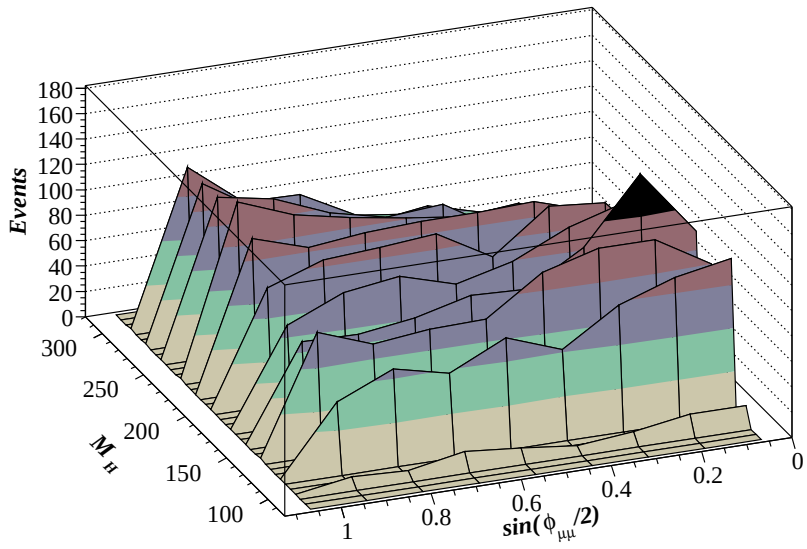

Figure 4.2: Angular separation of the muons in the $H \rightarrow WW$ signal events, as they change with the Higgs mass (generated with MC@NLO).

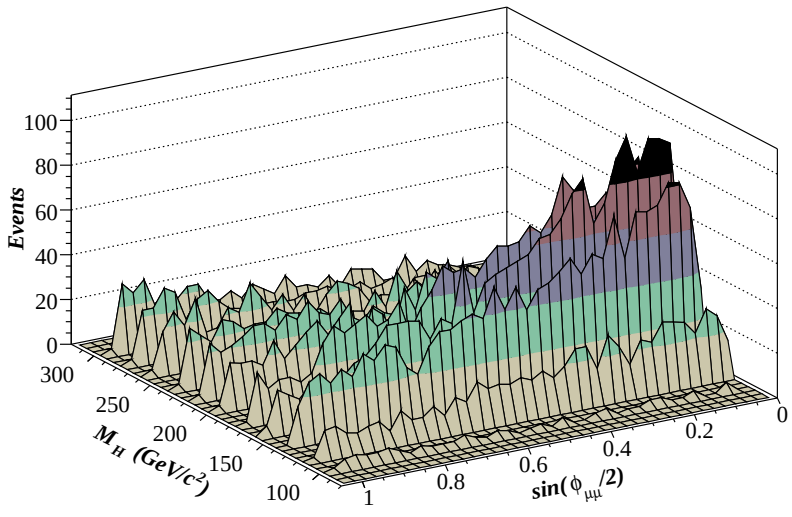

Figure 4.3: Angular separation of the muons in the $H \rightarrow WW$ signal events, as they change with the Higgs mass (generated with PYTHIA).

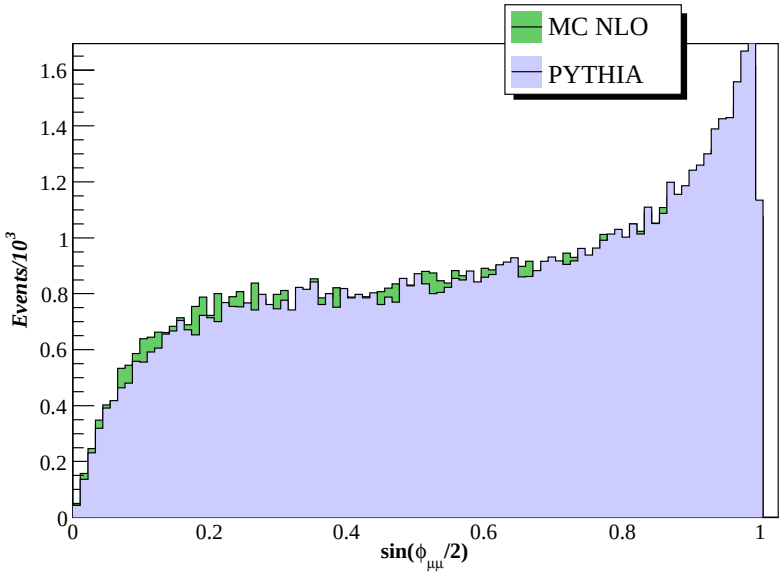

Figure 4.4: Angular separation of the muons in background events. The plotted MC@NLO and PYTHIA results show an equivalence in the two calculations.

M_H (GeV/c^2)	120	140, 160, 180
Cuts	$\sin(\phi_{\mu\mu}/2) < 0.4$	$\sin(\phi_{\mu\mu}/2) < 0.3$
	$M_{\mu\mu} < 50$	$20 < M_{\mu\mu} < 80$
	$10 < p_T^{\ell\max} < 46$	$30 < p_T^{\ell\max} < 55$
	$20 < \not{E}_T < 80$	$40 < \not{E}_T < 80$

Table 4.4: Kinematic cuts by Higgs mass subranges

the invariant mass spectrum is. Quantitively, search routines for the kinematic cut that optimized the SNR were programmed, looking in the variables of lepton pair angular separation and invariant mass, with the result that the event rejection ratios for both the signal and background processes were essentially equal, which does not get us any closer to enhance the SNR, but simply to lose statistics with each applied cut. Such effect can be qualitatively appreciated by taking a glance at figures 4.5, 4.6 and 4.7.

We now attemp to uncover the signal from the signal+background set. In view of the previous reflections, the range $200 < M_H < 300$ (GeV/c^2) is not evaluated. In the tables 4.5 and 4.6 we summarize the results. By default, it should be understood we evaluate the cuts and the corresponding statistics on the NLO data set, unless otherwise stated.

From the numbers in the tables we can observe the cuts rejected most of the background events, along with the signal ones too, and as a result, the greatest SNR achieved

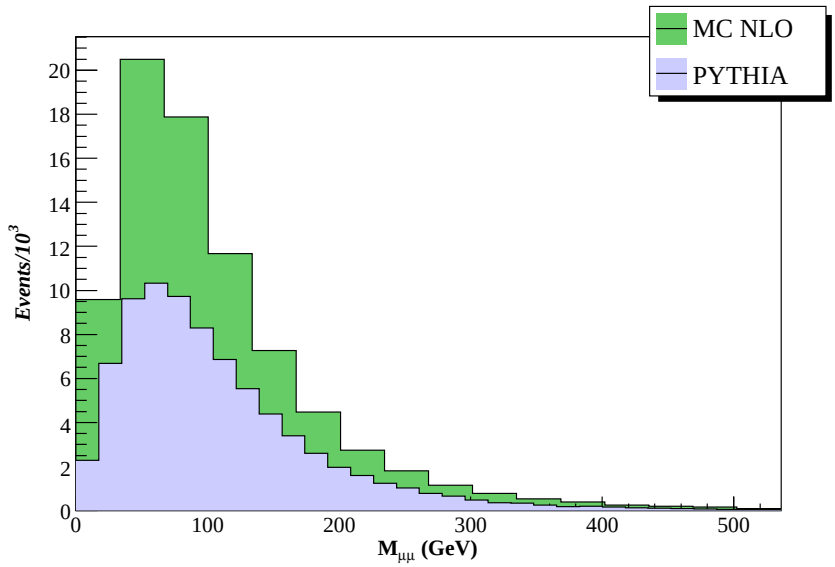

Figure 4.5: Muon pair invariant mass, background processes. MC@NLO and PYTHIA results are plotted together for comparison.

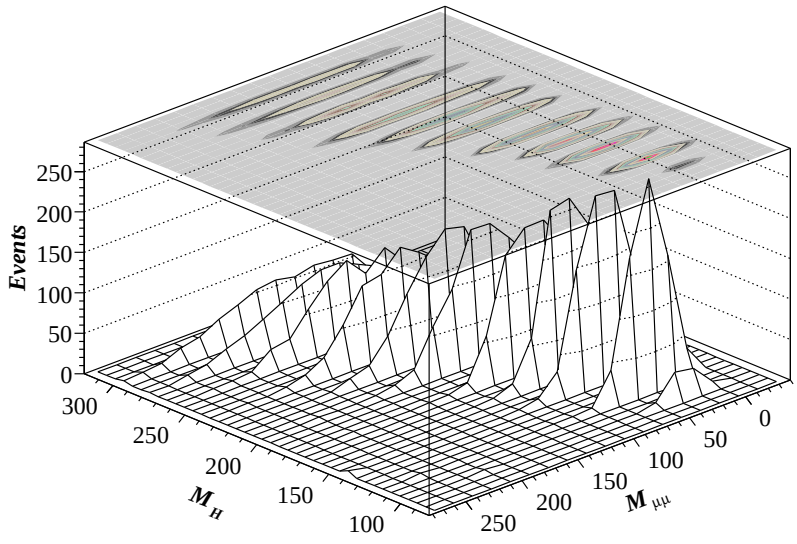

Figure 4.6: Muon pair invariant mass, signal processes, varying with the Higgs mass (generated with MC@NLO).

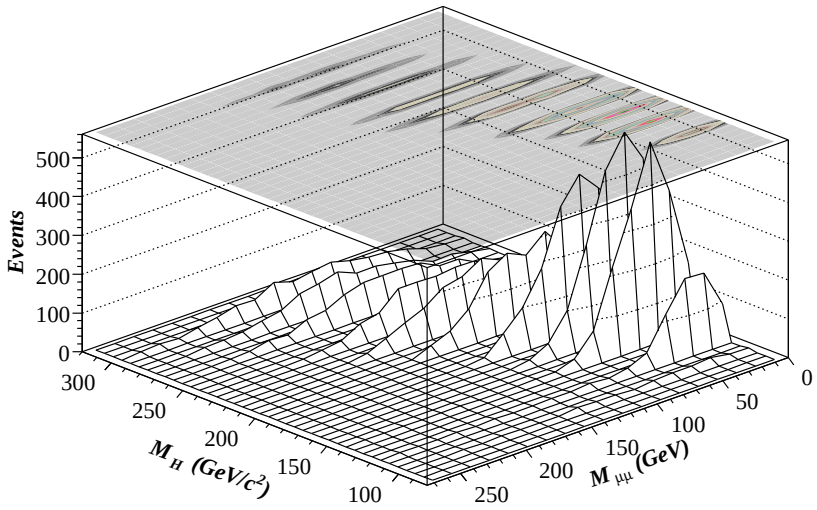

Figure 4.7: Muon pair invariant mass, signal processes, varying with the Higgs mass (generated with PYTHIA).

	QCD $\rightarrow WW$	$H \rightarrow WW$ M_H= 120($\mathrm{GeV/c^2}$)	$H \rightarrow WW$ M_H= 140($\mathrm{GeV/c^2}$)
ϵ_{tot}	$1.45 \cdot 10^{-2}$	8.385	11.875
Rel. S/R	-	$4.36 \cdot 10^{-2}$	$8.22 \cdot 10^{-2}$

Table 4.5: Number of expected events due to the effect of the cuts. The value of ϵ_{tot} indicates the fraction of filtered to unfiltered events, and below the SNR is shown.

is 0.1 for Higgs mass of 160 $\mathrm{GeV/c^2}$. The next step taken was the submission of these events into the neural network, but due to the low available statistics, the neural network was not succesful in effectively discriminating the signal events, and so they got lost within the ”sea” of background events not rejected. As an illustration of this outcome, the response of the network to the filtered events for a Higgs mass $m_H = 160$ $\mathrm{GeV/c^2}$is displayed in Figure 4.8. The layout of the network is the shown in Figure 3.1.

A similar study was done in [14], where they also get the same qualitative behavior for the SNR, which is to be maximum around the point m_H = 160 $\mathrm{GeV/c^2}$. For that study, a jet analysis is also undertaken, so that they are able to add a jet veto by which they can succesfully reject most of the dominating background, which is $t\,\bar{t}$ pair production (9% surviving events with the sole jet veto criterion). The conclusion that follows this realization is that this channel requires the analysis of the accompanying jets in order to gain discriminant power.

	$H \rightarrow WW$ M_H= 160($\mathrm{GeV/c^2}$)	$H \rightarrow WW$ M_H= 180($\mathrm{GeV/c^2}$)
ϵ_{tot}	15.52	10.5
Rel. S/R	0.10	$7.26 \cdot 10^{-2}$

Table 4.6: Continuation of Table 4.5.

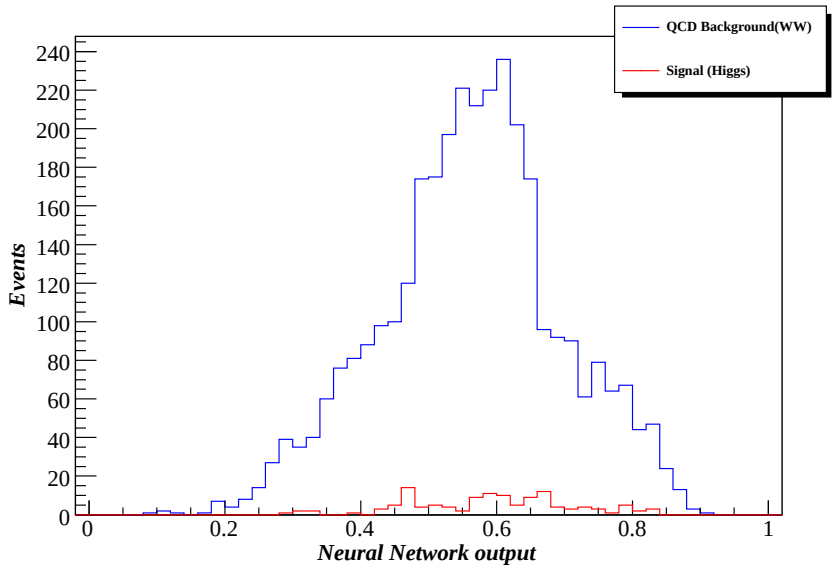

Figure 4.8: Neural Network output for the filtered data set corresponding to m_H = 160 $\mathrm{GeV/c^2}$. Clearly there is no gain at all in discriminant power.

4.3.2 The channel $H \rightarrow Z^0Z^0 \rightarrow 4\mu$

This is the so-called "gold plated" channel for the Higgs discovery, as the totality of its final state is detectable, it offers the possibility to measure directly the Higgs mass and has small backgrounds. However its cross section is low (about 3% of the Higgs production cross section), and because of specializing the analysis only to muonic final states the statistical count is lower and so more integrated luminosity is necessary to obtain statistically meaningful limits on observables. In spite of this, this channel is so special that even with the low statistics corresponding to our choice of integrated luminosity, a few events are enough to give us a signal. To get started, consider the figures 4.9, 4.10 and 4.11. The invariant mass spectrum of the 4 detected muons is shown, produced by the decay of the two Z^0 bosons, generated by the background process.

First fact at sight is the difference between the NLO and LO calculations of MC@NLO and PYTHIA for the low invariant mass range from 100 GeV to 200 GeV. Where in this range there are no events for the NLO data set, there are a few for the LO set. Nevertheless, these additional events, for all evaluated Higgs masses within this range,

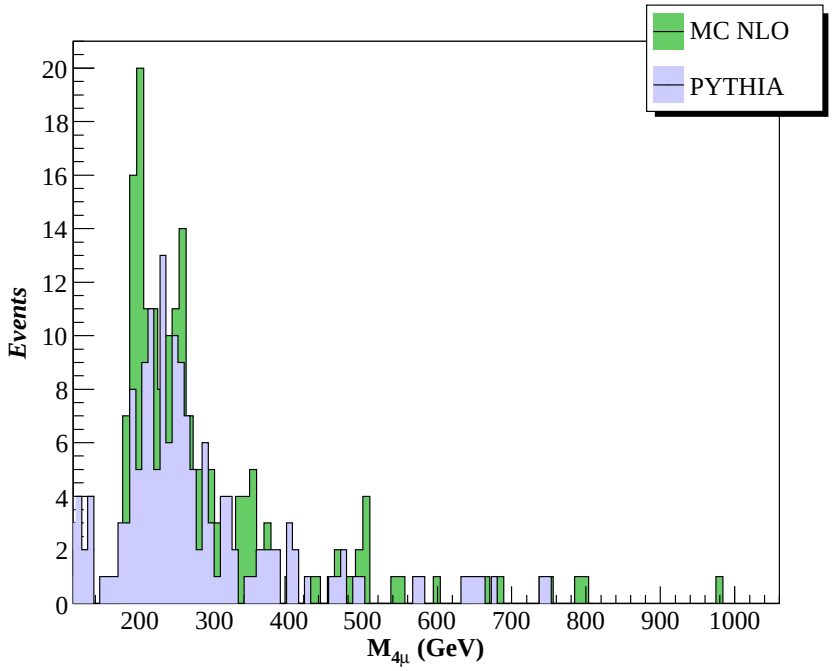

Figure 4.9: 4-muon invariant mass spectrum for the background process. MC@NLO and PYTHIA results are plotted together for comparison.

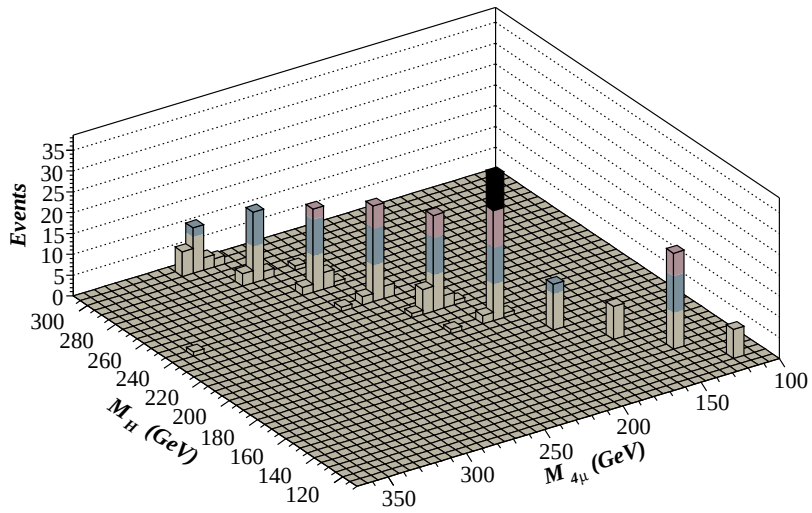

Figure 4.10: 4-muon invariant mass spectrum for the signal (generated with MC@NLO).

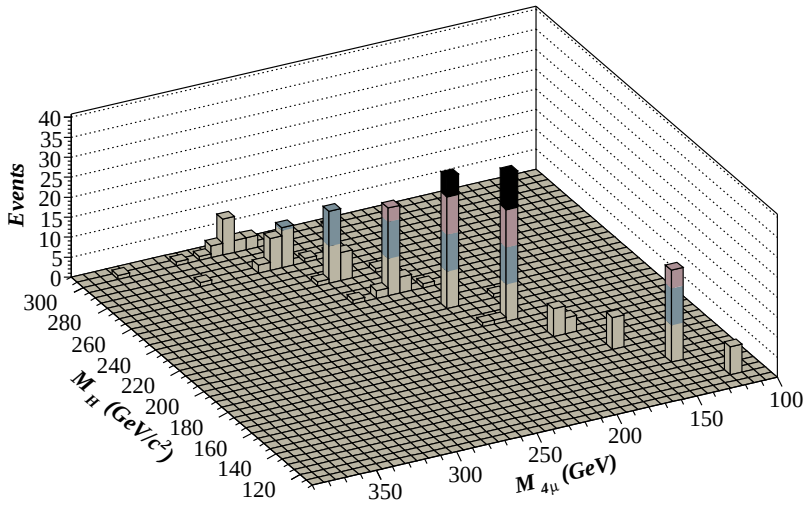

Figure 4.11: 4-muon invariant mass spectrum for the signal (generated with PYTHIA).

are outnumbered by their Higgs signal counterparts (for $m_H = 120\ \mathrm{GeV/c^2}$, there are 7 to 4 events, for $m_H = 140\ \mathrm{GeV/c^2}$, the ratio is 23 to 1, etc.), and so the SNR is kept higher than 1 for the whole range of Higgs masses. This confirms the this channel as the most promising among the rest for a Higgs signal discovery. However, as we mentioned earlier, a higher integrated luminosity is needed in order to be able to obtain meaningful results for discovery or exclusion. Exclusion in this channel would be signaled by the absence of an excess of events throughout the full mass range, specially for masses below 200 $\mathrm{GeV/c^2}$, where most of the theoretical and experimental estimates have placed their bets on. On the side of the angular distributions, the observed pattern for the signal and backgrounds is a rather isotropic distribution, out of which no useful criteria could be inferred; nonetheless, it is also true that the low event count sweeps out any possibility to observe variables with non-trivial behaviors, and so at this point no meaningful conclusions can be drawn from the angular distributions.

Final Comments

In this thesis work, we explored the discovery possibilities for a Standard Model Higgs boson of intermediate mass, as there are strong reasons that constrain its mass below the 300 GeV threshold. We studied the dominant decay modes, which are also the most useful ones as experimental signatures, as their leptonic final states are generally well distinguishable among the overwhelmingly large hadron content resulting from the collision of hadrons. It was noticed that the decay into W bosons provides discovery potential for Higgs masses around 160 GeV ($\pm$ 20 GeV approximately). The best channel, the decay into Z bosons, presents a clean signature, with low backgrounds throughout the considered range of Higgs masses. However, this channel needs a rather high integrated luminosity in order to be able to confirm a discovery, and so the $H \rightarrow WW$ channel is more suitable for a Higgs discovery in the aforementioned range. For this to be effective, we've shown it is absolutely necesary to study the jets associated with the process, as they constitute a powerful rejection criterion for the background processes. The use of neural networks may improve the signal to noise ratio, but only if and once it becomes reasonably low for the noise statistics to favor or at least be equal to the signal data, so the cut-based approach is still of fundamental importance. The use of Neural Networks was explored as a complement to our cut-based approach, but it proved unsuccessful. It is expected, in view of the cited articles (in particular [14]), that the study of the jets remaining from the collisions provides a criterion with high background rejection power and almost no impact on the signal event count. For jet studies, neural networks show great functionality[3], and so this becomes path for further exploration in this topic.

Bibliography

[1] *ROOT - An Object Oriented Data Analysis Framework*, volume 389, 1997.

[2] V. A. Bednyakov, N. D. Giokaris, and A. V. Bednyakov. On Higgs mass generation mechanism in the Standard Model, 2007.

[3] Gregorio Bernardi, C. D. F. Collaboration, and D. 0. Collaboration. Searches and Prospects for the Standard Model Higgs boson at the Tevatron, 2006.

[4] CDF and D∅Collaborations. Results of the Tevatron Higgs Sensitivity Study. *FERMILAB-PUB-03/320-E*, 2003.

[5] The CDF Collaboration. Search for $H \to WW^*$ Production with Matrix Element Methods at Tevatron Using 1.9 $\mathrm{fb}^{-}1$ Data. Technical report, 2007.

[6] The D∅ collaboration. Search for the Higgs boson in $H \to ll'$ $(l, l' = e, \mu)$ decays with 1.7 $\mathrm{fb}^{-}1$ of data at D∅. 2007.

[7] The LEP Collaborations: Aleph collaboration, D. E. L. P. H. I. Collaboration, L. 3. Collaboration, O. P. A. L. Collaboration, and the LEP Electroweak Working Group. A Combination of Preliminary Electroweak Measurements and Constraints on the Standard Model, 2006.

[8] G. Corcella, I. G. Knowles, G. Marchesini, S. Moretti, K. Odagiri, P. Richardson, M. H. Seymour, and B. R. Webber. *JHEP*, (0101):10, 2001.

[9] Christopher Delaere. TMultiLayerPerceptron: Designing and using Multi-Layer Perceptrons with ROOT, 2004.

[10] Christopher Delaere. *Study of WW decay of a Higgs boson with the ALEPH and CMS detectors*. PhD thesis, 2005.

[11] John Ellis, Giovanni Ridolfi, and Fabio Zwirner. Higgs Boson Properties in the Standard Model and its Supersymmetric Extensions, 2007.

[12] S. Frixione, P. Nason, and B. R. Webber. Matching NLO QCD and parton showers in heavy flavour production. *JHEP*, 0308:007, 2003.

[13] S. Frixione and B. R. Webber. Matching NLO QCD computations and parton shower simulations. *JHEP*, 0206:029, 2002.

[14] M. Dittmar G Davatz and A. S. Giolo-Nicollerat. Standard Model Higgs discovery potential of CMS in the H $\rightarrow$ WW $\rightarrow \ell\nu\ell\nu$ channel. *Journal of Physics G: Nuclear and Particle Physics*, 34(3):–85, 2007.

[15] Masaharu Goto. C++ Interpreter - CINT.

[16] David Griffiths. *Introduction to Elementary Particles*. 1987.

[17] S. Eidelman et al. (Particle Data Group). Searches for Higgs bosons. *Phys. Lett. B 592, 1*, (partial update for edition 2006), 2005.

[18] F. Halzen, A. D. Martin, and N. Mitra. Quarks and Leptons: An Introductory Course in Modern Particle Physics. *American Journal of Physics*, 53:287–287, mar 1985.

[19] G. Marchesini, B. R. Webber, G. Abbiendi, I. G. Knowles, M. H. Seymour, and L. Stanco. 1992.

[20] J.B. TauskE-mail The Corresponding Author R. BoughezalE-mail The Corresponding Author and J.J. van der BijE-mail The Corresponding Author. Three-loop electroweak corrections to the W-boson mass and $\sin\theta_{\mathrm{eff}}^{\mathrm{lept}}$ in the large Higgs mass limit. *j.nuclphysb.2005.07.013* , 2005.

[21] Torbjorn Sjostrand. Monte Carlo Generators for the LHC, 2005.

[22] Torbjorn Sjostrand, Stephen Mrenna, and Peter Skands. *PYTHIA 6.4 Physics and Manual*, 2006.

[23] Michael Spira. QCD Effects in Higgs Physics. 1997.